Stochastic Spiking Behavior in Neuromorphic Networks Enables True Random Number Generation

Susant K. Acharya,[†,§] Edoardo Galli,[†,§] Joshua B. Mallinson,[†] Saurabh K. Bose,[†] Ford Wagner,[†] Zachary E. Heywood,[‡] Philip J. Bones,[‡] Matthew D. Arnold,[¶] and Simon A. Brown[*,†]

†*The MacDiarmid Institute for Advanced Materials and Nanotechnology, School of Physical and Chemical Sciences, Te Kura Matū, University of Canterbury, Private Bag 4800, Christchurch 8140, New Zealand*

‡*Electrical and Computer Engineering, University of Canterbury, Private Bag 4800, Christchurch 8140, New Zealand*

¶*School of Mathematical and Physical Sciences, University of Technology Sydney, PO Box 123 Broadway NSW 2007, Australia*

§*S.K.A. and E.G. contributed equally to this paper.*

E-mail: simon.brown@canterbury.ac.nz

Abstract

There is currently a great deal of interest in the use of nanoscale devices to emulate the behaviors of neurons and synapses, and to facilitate brain-inspired computation. Here it is shown that percolating networks of nanoparticles exhibit stochastic spiking behavior that is strikingly similar to that observed in biological neurons. The spiking rate can be controlled by the input stimulus, similar to 'rate coding' in biology, and the distributions of times between events are log-normal, providing insights into the atomic-scale spiking mechanism. The stochasticity of the spiking behavior is then used for true random number generation and the high quality of the generated random bit-streams is demonstrated, opening up promising routes towards integration of neuromorphic computing with secure information processing.

Keywords

Neuromorphic, percolation, spiking neurons, stochasticity, true random number generation

1 Introduction

Neuromorphic or 'brain-like' computing seeks to overcome the limitations of the conventional Von Neumann architecture by physically emulating the basic building blocks of biological brains — that is neurons and synapses — at small circuit or device level.[1,2] Such an approach could potentially provide the capabilities of biological perception and cognitive information processing within a compact and energy-efficient platform, thereby enabling, for example, processing of data directly on-chip in so-called edge computing applications.[3] Synaptic functions have been scalably and efficiently emulated using memristors,[4] memtransistors,[5] multi-gated transistors,[6] and phase-change memory devices.[7] Emulation of spiking neurons has traditionally relied on circuits comprising multiple transistors[8–10] but attempts to take advantage of the small size and low power consumption of emerging nano devices are now underway. Recent demonstrations include: the 'neuristor', built using two nanoscale Mott memristors;[11,12] leaky integrate-and-fire neurons, based on memristors coupled with either CMOS transistors,[13] Mott insulators,[14] or capacitors;[15] and stochastic neurons using phase-change materials.[16] Other functions of biological neurons that have been tentatively demonstrated include periodic spiking and oscillations[11,17] and rate coding of stimuli.[18] However, many challenges remain. In particular, it is important to develop individual devices that capture the full range of dynamics of biological neurons.[12] Ref. 16 so far appears to be the only report of a single nano device which replicates the stochastic firing characteristics of biological neurons.

Biological neurons exhibit inherently stochastic behavior.[19–21] The source of stochasticity can be attributed to numerous complex phenomena that take place at the molecular level, such as stochastic gating of ion channels in neurons, chaotic motion of charge carriers due to thermal noise, synaptic fluctuations, inter-neuron morphological variability, and the effect of background noise.[16,22,23] Stochasticity is important because it aids noise-tolerant and energy-efficient signal coding and transmission,[20] tunes the degree of synchrony between neurons, and enhances sensitivity to environmental stimuli.[19,21] Stochastic behavior

is at the heart of bio-inspired computation and, for example, 'stochastic facilitation'[21] allows complex computational tasks to be performed that are too computationally intensive for conventional hardware.[23] These tasks include Bayesian inference,[24] deep learning,[25] and non-deterministic polynomial-time (NP) hard problems such as intrinsic optimization[26] and Boolean satisfiability.[27] Stochasticity has been exploited in a dot product engine[28] and combinatorial optimization.[29]

Stochasticity is also an important factor in secure information processing and transmission.[30] In particular, efficient random number generation is required for a wide range of applications such as encryption and cryptography,[31] simulations,[32] and stochastic computing.[33] Pseudorandom number generators (PRNGs) are commonly available in standard software packages, but are actually intrinsically deterministic.[34,35] PRNGs are therefore usually not suitable for security applications, where it is vital that a sequence of random numbers cannot be reproduced. True random number generators (TRNGs) are devices that exploit intrinsic stochasticity in physical phenomena to generate high quality random bit-streams[31] that are secure from external parties. As higlighted in Ref. 30, integration of TRNGs into emerging computing paradigms would enable new approaches to secure information processing and might, for example, allow some tasks to be performed directly within memory, thereby bypassing the von Neumann bottleneck.

Here we show that percolating networks of nanoparticles (PNNs)[36,37] can be used to generate stochastic spiking behavior that is similar to that of individual biological neurons. The spiking behavior emerges when the devices are measured on fast timescales (1 - 10 μs). We show that the intervals between events have log-normal distributions, originating from intrinsically probabilistic atomic-scale switching processes. We show that the atomic-scale dynamics allow reproduction of some of the basic functionality of biological neurons: stochasticity, rate coding of information, and serial correlations. Finally, we show that the inherent stochasticity in our nanoparticle devices can be exploited for true random number generation with high bit rates and bit-streams that pass standard benchmark tests without
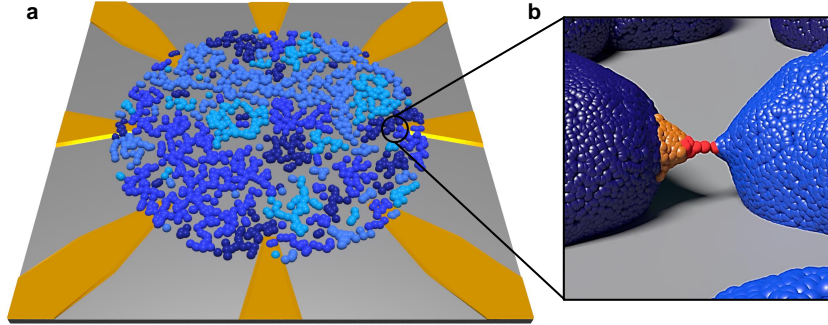
Figure 1: Percolating network of nanoparticles and atomic-scale switching process. (a) Schematic showing multi-terminal device geometry (contacts shown in yellow) with deposited PNN. Groups of connected particles are shown in different shades of blue. (b) Schematic of a tunnel gap within the nanoparticle network showing formation of an atomic-scale filament. The filament starts to form as a hillock (orange atoms) on one side of the tunnel gap due to the potential difference across the gap. Once the filament is formed (red atoms), the new Ohmic connection allows significantly higher current to flow through the filament, leading to its eventual destruction. Note that the filament is atomic scale and the nanoparticles are $\sim$ 20 nm in size.[36,38]

the need for post-processing.

1.1   Percolating Networks of Nanoparticles

Complex networks of nanomaterials have recently emerged as promising systems for neuro-morphic computing.[36,37,39–43] In particular it has been shown that PNNs (Figure 1a) exhibit complex patterns of correlated electrical signals that are similar to those of networks of biological neurons in the cortex.[37] The origin of this behavior is that the percolating networks contain many tunneling gaps (between groups of well-connected nanoparticles) which each emulate biological neurons. Atomic-scale switching processes in each tunnel gap are illustrated in Figure 1b – note that the deposition process leads to voids between particles[38,44] and that (in contrast to some other types of atomic switch[45]) it is believed that there is no dielectric material in the gaps. The switching processes involve formation and destruction of atomic-scale filaments[44] in these gaps and capture some of the integrate and fire characteristics of biological neurons.[38] When one switch changes state, consequent changes in the

distribution of voltages/currents through the network lead to other switching events, and hence to avalanches of switching events. The observed avalanches of electrical signals are consistent with critical states, which are associated with optimal information processing.[36] The critical dynamics in fact result from the combination of integrate and fire dynamics together with the scale-free topology of the percolating network.[37,38]

Previous work relied on measurement techniques that were limited to millisecond sampling intervals[36–38] and the behavior of the networks at shorter time scales has so far not been investigated. Therefore questions such as whether correlated avalanching behavior continues to be observed at faster sampling intervals, or what might be the ultimate limits for operation of neuromorphic devices based on these networks remain unanswered. Here we show that the novel single 'neuron' spiking behavior that is the focus of this work emerges at microsecond timescales.

2   Results and Analysis

Our percolating networks of nanoparticles were deposited on insulating substrates and contacted by multiple electrodes, which were pre-fabricated using optical lithography techniques. Sn nanoparticles were deposited until the onset of conduction (percolation threshold) was reached, which ensures the necessary complex network of switching sites (tunnel gaps).[36] Optical images of the devices and SEM images of the morphology of the nanoparticle network are shown in Figure S1. The devices were measured with a high speed measurement system that allows signals from up to 16 electrodes to be recorded at MHz sampling rates. All results presented here are obtained using DC inputs. Details are provided in the Methods section below. Figure 2a shows complex patterns of switching events in the current measured from one electrode of a typical device. The current varies around a constant mean value and the devices exhibit the same behaviour (both qualitatively and quantitatively) over periods of months.[46] Figure 2b shows that the distribution of inter-event intervals (IEIs) is
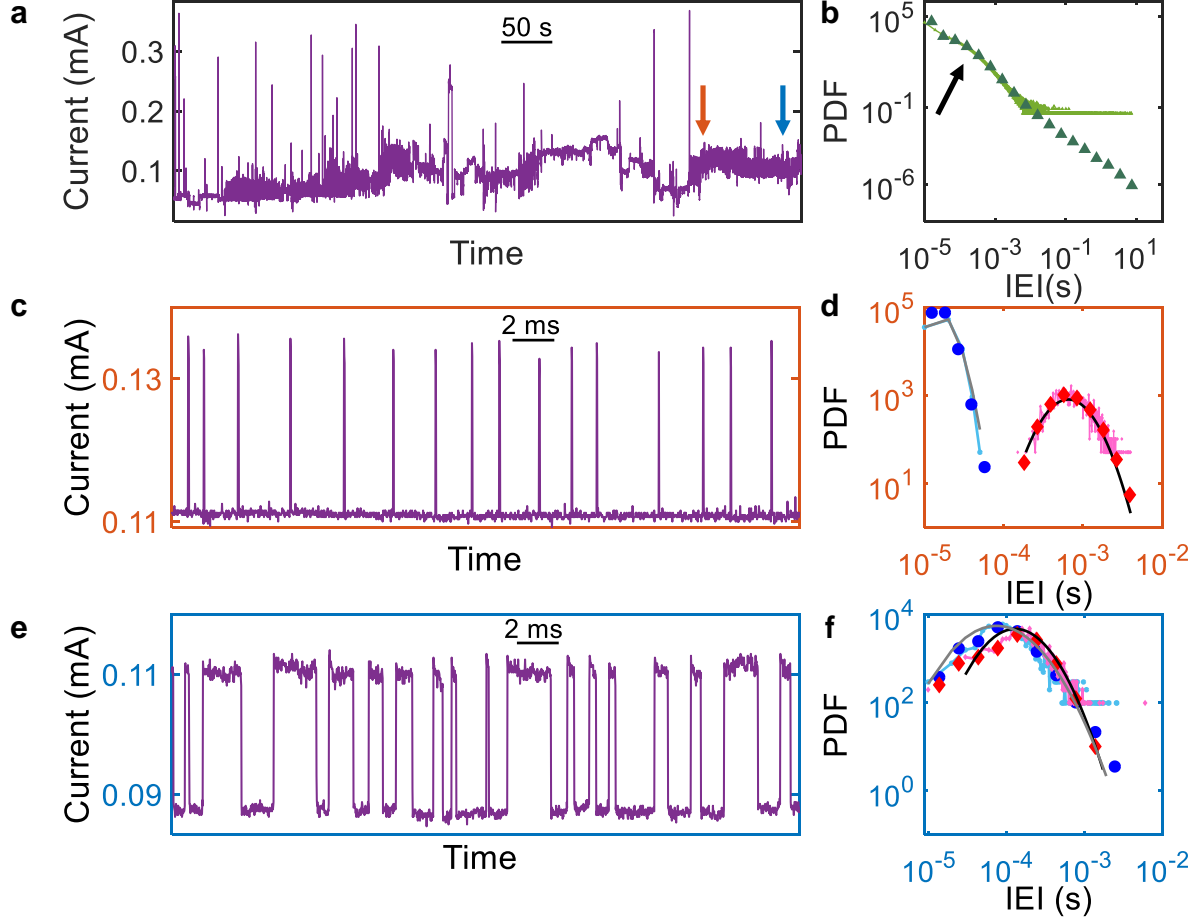
Figure 2: Spiking behavior in a single tunnel gap, stochasticity, and log-normal dynamics. (a) Typical example from Device 1 of long term switching activity with complex patterns of switching events occurring throughout the network. Applied DC voltage is 8V and sampling interval is 10 μs. (b) Probability density function (PDF) of the inter-event intervals calculated from the whole network activity shown in panel a. The additional peak (arrowed) corresponds to the spiking behavior shown in panels c and e. The underlying power law behavior is associated with correlated avalanches[36,37] (see Figure S2). Light and dark green triangles are PDFs obtained using linear and logarithmic bins, respectively. (c and e) Zoomed in portions of panel a indicated by the orange and cyan arrows, showing examples of spiking activity generated by single tunnel gaps and characterized by two distinct current levels. The time scale is 25000 times smaller than the one in panel a. t_U and t_D represent the time spent in the UP or DOWN states, respectively. In panel c (orange border) $t_U <<$ t_D while in panel e (cyan border) $t_U \sim t_D$. (d and f) PDFs of the inter-event intervals for the segments of data shown in panels c and e. Cyan/blue circles and pink/red diamonds are PDFs obtained using linear/logarithmic bin sizes for t_U and t_D, respectively. t_U and t_D follow log-normal distributions. Log-normal maximum likelihood (ML) fits are shown as the gray and black lines.

7

approximately a power law over more than six orders of magnitude in time, with a power law exponent of ~1.8 similar to that reported previously in two electrode devices at much slower sampling rates[37] (the arrowed feature is discussed below). More detailed analysis (see Figure S2) shows that the avalanches of events are consistent with criticality, with similar power-law size and duration distributions to those observed previously.[36,38]

Figures 2c and e show that it is possible to identify periods during which the changes in current are the same for *every* event, with increases (decreases) in current corresponding to formation (destruction) of the *same* atomic-scale filament (further examples are shown in Figures S3 and S4) *i.e.* within the same tunnel gap. We emphasise that each different spike train (for example Figures 2c and e) originates from a different tunnel gap. The key new feature of the data is that on very short timescales the *same* switching events are often observed *repeatedly*. Note however that the IEIs are not constant *i.e.* they are *intrinsically stochastic*.

Figure S5a shows the distribution of the current measured in the two states of the switch (UP and DOWN, corresponding to high and low currents respectively) and fits to the distributions are shown in Figures S5b and c. When the filament is absent a narrow normal distribution of currents is observed, with the width of the distribution corresponding to the measurement noise. When the filament is formed, the current has a broader distribution: the current flowing is more variable due to stochastic variations in the filament structure on the atomic-scale, as discussed in more detail in 'Mechanism' Section.

Depending on the lifetime of the filament the observed behavior can appear as either a sequence of well-defined spikes or as a sequence of steps between two current levels. The latter behavior appears similar to Random Telegraph Noise (RTN), but RTN is usually associated with charge transport in 2-level systems and leads to exponential statistics which are very different to those observed here.[47] The times spent in each state (t_U and t_D) follow log-normal distributions (Figures 2d and f). When spike-like behavior is observed (Figure 2c) the centers of the log-normal distributions of t_U and t_D are clearly different (Figure 2d),

whereas they are similar during RTN-like behavior (Figure 2f). The difference between the two cases is simply the difference in the average lifetime of the atomic filament, and so we use the term 'spiking' to describe both. This spiking behavior is responsible for the deviation from a pure power-law at short IEIs in the histogram in Figure 2b (arrowed) and was not clearly resolved in previous measurements at slower sampling speeds.[36,37] The log-normal distributions obviously represent the stochastic behavior that is visible in Figures 2c and e.

As noted above, stochasticity is an important property of biological neurons, and indeed log-normal behavior is sometimes observed for single neurons.[48] Table S1 summarizes data from multiple examples of spiking for many datasets, devices, and applied voltages. Each dataset corresponds to a different spike train (for example Figures 2c and e) originating from a different tunnel gap within a network. The observed t_U and t_D distributions are always log-normal, but their average values (τ_U and τ_D, respectively, calculated from the log-normal ML estimators) can both vary over several orders of magnitude – see discussion in 'Mechanism' Section.

Figure 3a shows an example of a typical spike train observed over a long period at a constant applied voltage, highlighting occasional long intervals between spikes. These occur because log-normal distributions are *heavy-tailed*:[51] relatively long intervals between events, in fact up to two orders of magnitude longer than the mean of the distribution, are observed quite often. Figure 3b shows qualitatively that there are *correlations* between successive inter-*spike*-intervals (ISIs) *i.e.* that long (short) ISIs tend to follow other long (short) ISIs. (Note that each ISI is the time between rising edges *i.e.* the sum $t_U + t_D$; ISI $\neq$ IEI. Long (short) ISIs are defined to be those that are longer (shorter) than the mean ISI, see Figure S6.) Figures 3c and d make these correlations more quantitative by plotting the relationship between successive ISIs for 25 different data segments (each with a different colour). See caption for details. In Section II of the Supporting Information we explain that (i) these serial correlations are important features of the behavior of biological neurons and (ii) the observed positive serial correlations are driven by the modulating effect of slow changes in
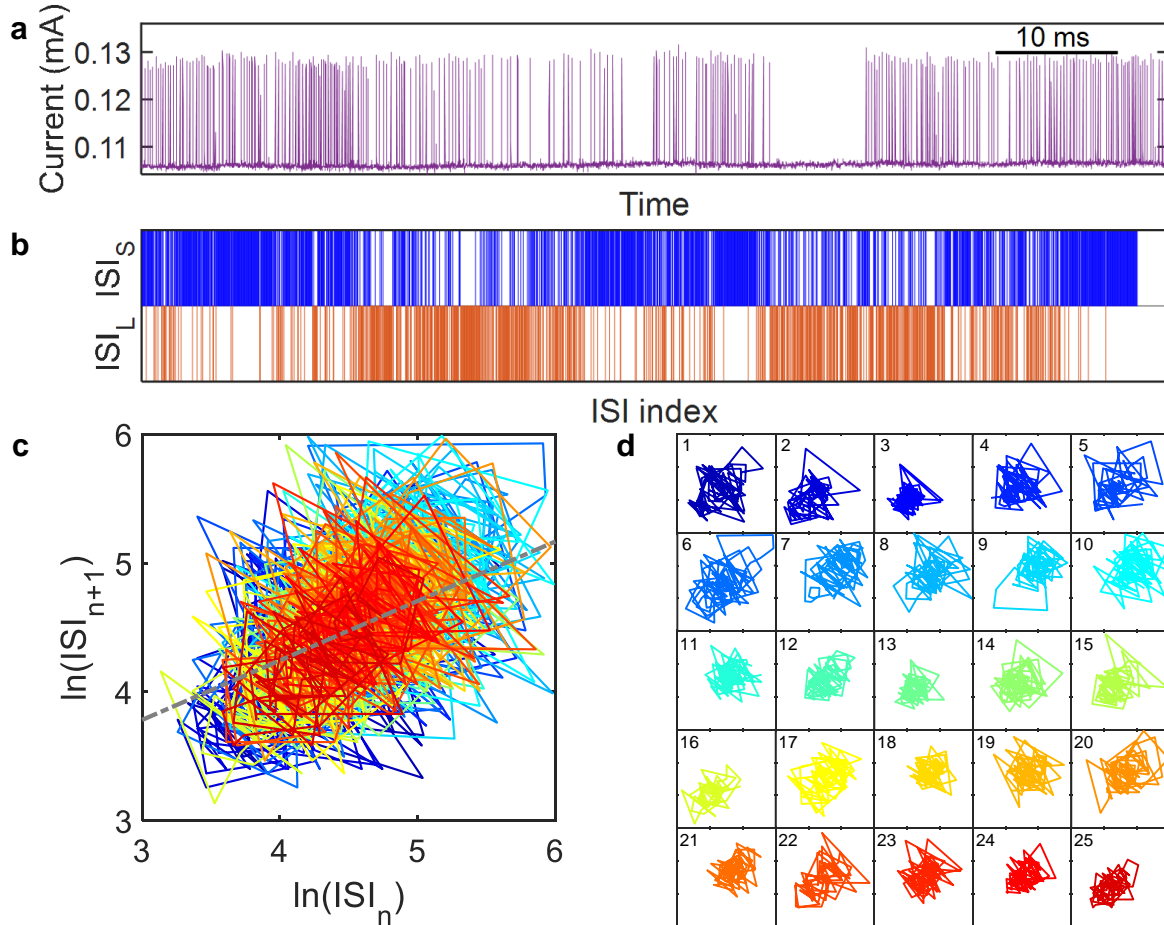
Figure 3: Stochasticity and serial correlations. (a) Current measured from Device 1 showing irregular and stochastic spiking activity. (b) Patterns of short and long ISIs, ISI_S and ISI_L, showing that long and short ISIs tend to be grouped together. This is indicative of the existence of positive serial correlations which are often observed in the ISI sequences of biological neurons.[49] The mean ISI is used as a threshold to define ISI_S and ISI_L as shown in Figure S6. (c) Return map[50] of the consecutive ISIs for the same dataset. 25 different data segments are shown using different colours. Note the logarithmic scales. A strong positive serial correlation is clearly visible *i.e.* the return map shows that a long ISI tends to be followed by another long ISI and correspondingly, a short ISI is followed by another short ISI. The slope of the linear regression (dashed gray line, slope = 0.46) estimates the serial correlation coefficient for sequential ISIs across the whole dataset. (d) Time evolution of the return map for the 25 different data segments (dark blue to dark red) shown in panel c. Each square panel contains 80 ISIs. The x and y scales of each square panel are identical to those in panel c. Note that the fitted line in panel c represents the average serial correlation for the *whole* dataset. Panel d shows that there are a number of contributions to the overall correlation: (i) very strong serial correlations in some data segments (steep slopes such as in panels 1, 6, and 22), (ii) weaker correlations (circular clusters of data points such as in panels 11, 13, and 18) and (iii) variation of the position of the center of each cluster of data points for different panels. The scatter in each panel is consistent with the stochasticity of the observed spiking. The clustering of the data in the return maps suggests the existence of faster and slower modes of spiking behavior.

10

potential at other tunnel gaps in the network.

2.1 Control by Electrical Stimuli

The spiking behavior shown in Figure 2 is typically observed in the current measured at a single electrode (*i.e.* it is either not observed simultaneously at other electrodes, or is observed only weakly). This suggests that spiking originates from a tunnel gap which is well-connected to that particular electrode. Long sequences of uninterrupted spikes are more easily observed in samples that have been subjected to long periods of high voltage stimulus, which can cause some other switching sites to be deactivated (high voltages ($\sim$10V) can cause irreversible local changes in morphology; a small increase in the size of a nanoscale tunnel gap can render it inactive). This eliminates complex avalanches that partially mask the spiking behavior, and hence facilitates detailed investigations of spiking and potential applications. When competing processes are deactivated, we are able to tune the spiking rate by controlling the applied voltage, as shown in Figure 4. When the voltage input to the device is tuned we observe a change in behavior from spiking (higher voltage, $V \sim$7.6V) to RTN-like ($V \sim$7.0-7.4V), to quiet (lower stimulus, $V \sim$6.8V). Spiking is still stochastic (with a log-normal distribution of t_U and t_D, Figure 4b) but the average spiking rate of this individual 'neuron' is controllable. This shows that the PNNs can encode information in the spiking rate (*i.e.* achieve 'rate coding') and have potential to be used as stochastic neuristors.[11,52]

Figure 4a shows that as the applied voltage is increased the time spent in the UP state is reduced and the number of spikes increases. In fact the rate of spiking increases approximately exponentially with applied voltage (Figure 4c). This is because of an exponential decrease in τ_U while τ_D remains approximately constant (Figure 4d – note that there is a much weaker, but still exponential, decrease in τ_D). Recall that τ_U corresponds to the average time taken to break the atomic-scale filament shown in Figure 1b (and τ_D is the time to form the filament). Hence the results in Figure 4 provide strong evidence that the rate at

11

which atomic-scale filaments are broken is exponentially dependent on the applied voltage, whereas the rate of formation of the filaments is substantially unaffected by voltage. (Note that according to Ohm's Law the current increases in proportion to voltage, so this in itself does not demonstrate a voltage-driven rather than current-driven mechanism – see further discussion below.) This exponential behavior is confirmed in Figure 4e where the slope of the plot is related to the difference in energy, ΔE_{UD}, between the atomic configurations in the UP and DOWN states.[47] More specifically the slope is $\Delta E_{UD}/(eE_{local})$, where E_{local} is the local electric field in the tunnel gap of interest. $E_{local} = \beta V_{applied}/d$, where d is the size of the gap and β captures the voltage dividing effect of the complex network. Unfortunately in general neither β nor d are known, and so it is not possible to determine ΔE_{UD}.

Figure S8 shows the variation of τ_U and τ_D for multiple examples of spiking and for several devices. As for the voltage-dependent data discussed in the previous paragraph, it is immediately apparent that τ_D is approximately constant while τ_U varies significantly (over five orders of magnitude). The strong sample-to-sample and example-to-example variation indicates that the time to break an atomic-scale filament depends on the local configuration of the network *i.e.* the position of the tunnel gap within the complex fractal architecture.[37] In contrast, the time to form the filament is much less sensitive to the local configuration. These data provide important insights into the atomistic mechanism responsible for spiking, as discussed in the next section.

We note finally that: (i) the main results of the analysis discussed above are independent of the type of curve fitting: Figure S7 shows the results of fitting exponentials to the data of Figure 4, as for a standard RTN analysis.[47] Table S1 shows fitted parameters for all spiking datasets analyzed – the trends are comparable for both the log-normal and exponential analyses. (ii) At high electric fields the switching speed (time to form/break an atomic-scale filament) is faster than $1\mu s$, see Figure S3, similar to the switching speeds observed for Ag/AgS atomic-scale switches in the high electric field regime.[45]
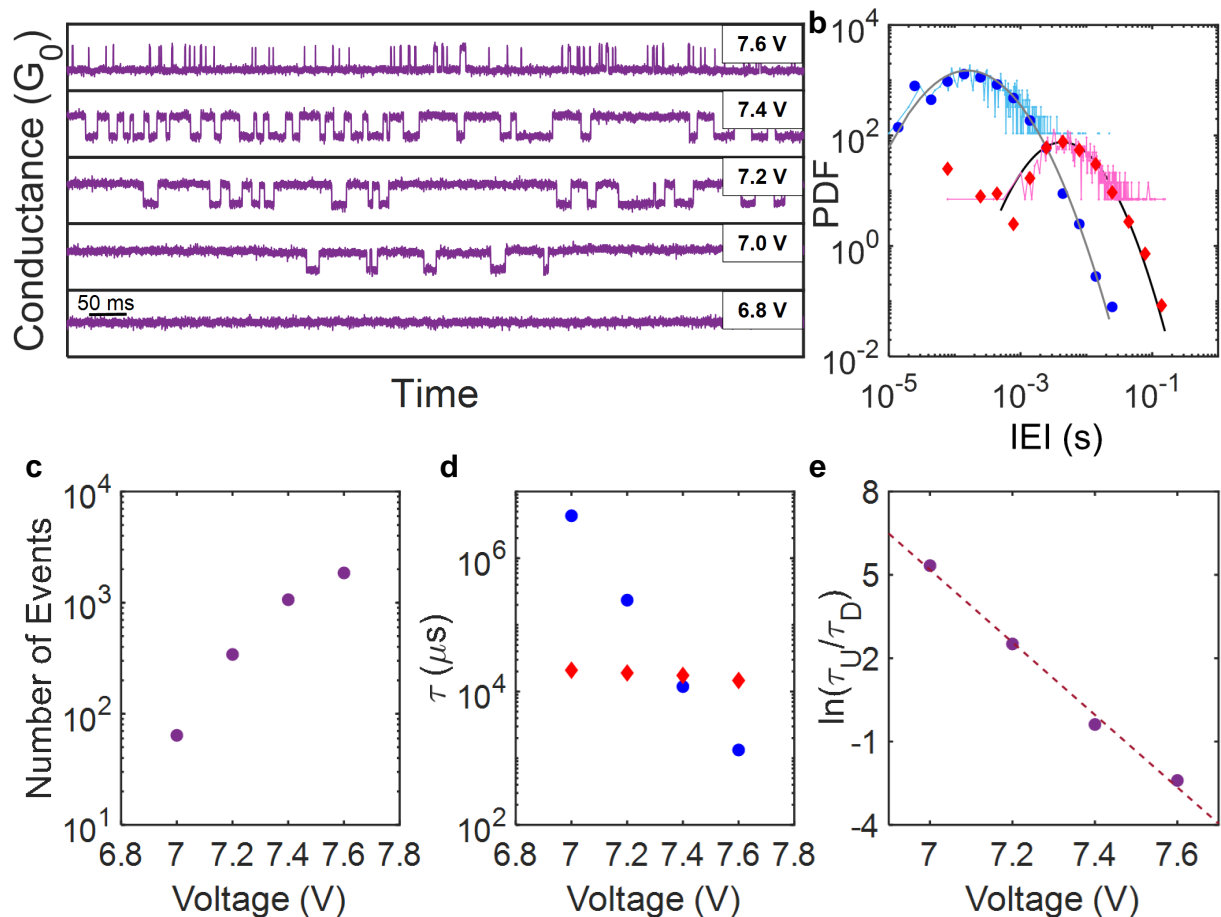
Figure 4: Spiking activity controlled by voltage stimulus, *i.e.* 'rate coding'. (a) Conductance of Device 3 measured at different applied voltages. The time spent in the UP state, t_U, decreases with increasing applied voltage. Sampling interval is 10 μs. The range of the vertical axis is 0.13 G_0 for each panel. [Note that conductance is used here instead of current in order to allow comparison of data obtained using different input voltages. Current increases with voltage according to Ohm's law.] (b) PDFs of the inter-event intervals of Device 3 at an applied voltage of 7.6 V. Cyan/blue circles and pink/red diamonds are PDFs obtained using linear/logarithmic bin sizes for t_U and t_D, respectively. Gray and black lines represent the log-normal ML estimates of t_U and t_D, respectively. (c) Number of events as a function of applied voltage during 15 s of spiking activity. Event count increases approximately exponentially with applied voltage. (d) Mean time τ_U (blue circles) and τ_D (red diamonds), calculated from the log-normal ML estimators, as a function of applied voltage. τ_U decreases with increasing applied voltage while τ_D appears approximately constant (there is a much weaker, but still exponential, decrease). (e) Logarithm of the ratio between τ_U and τ_D as a function of applied voltage. Note that this analysis is performed entirely using log-normal ML estimators, in contrast with the standard approach which is to assume that data such as that shown in panel b can be fitted with exponential functions.[47] The standard form of analysis is shown in Figure S7 for comparison.

13

2.2 Mechanism

Log-normal statistics (LNS) can result from any generic process involving a cascade of multiplicative conditional probabilities.[51] It has previously been shown that atomic hopping processes, which are governed by exponential Boltzmann probabilities, can lead to LNS during formation and destruction of *nanoscale* filaments.[53–55] These models typically describe movement of many atoms through an oxide matrix in order to form (comparatively large) filaments, and therefore describe fundamentally different switching processes. Nevertheless, we envisage that a similar hopping model could explain the motion of a small number of atoms across multiple atomic sites[56–58] near a tunnel gap – see schematic illustration in Figure 5a. In such a model the probability of formation of a filament would be a product of exponential probabilities of hopping between sites

$$P(E) = exp(-(U_i - E)/k_B T) \tag{1}$$

where U_i is the energy barrier for each hop and E is the energy supplied by the applied electric field or current. Such products would directly result in LNS.[51] However, a sequential hopping model does not seem to be compatible with the observed reversibility and repeatability of the switching process. Repeatability requires that the formation of subsequent filaments would be governed by the same sequence of hopping steps, but it seems very unlikely that once a filament has formed the displaced atoms would revert to their original positions (i.e. that the hopping process in Figure 5a would be perfectly reversed).

The reversibility that is evident in the data (Figure 2) indicates that it is much more likely that a single atom is responsible for spiking, with the atom jumping between two sites, or two similar sites, as illustrated in Figure 5b. The LNS would then result directly from a normal distribution of U (see Eq. 1), representing atomic-scale variations in the energy barrier (or pinning energy) each time the atom changes position. The fitted parameters shown in Table S1 support this interpretation since the widths of the distributions of t_U and
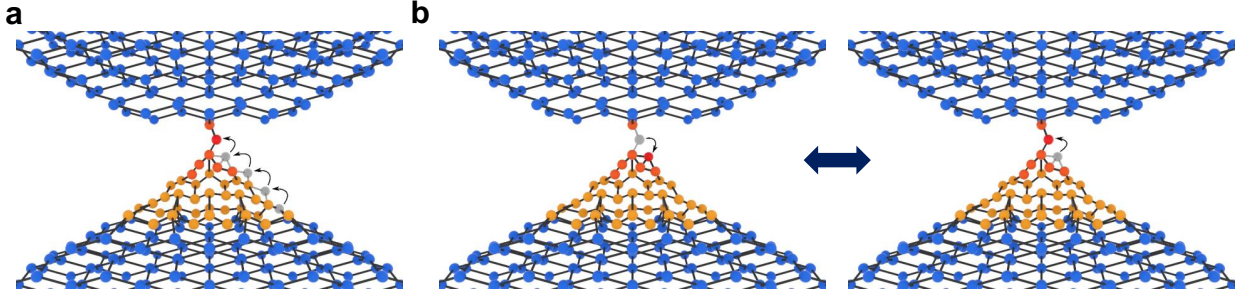
Figure 5: Schematics of two possible switching mechanisms that can lead to log-normal statistics. (a) Sequential hopping of an atom from site to site. LNS result from the multiplicative probability of the atom moving from the initial to the final site. (b) Direct hopping from an initial site to a nearby final site. LNS result from a distribution of pinning energies in the two sites. The colours of the atoms (blue, orange, and red) correspond to the particles, hillock, and the filaments shown in Figure 1. The moving / hopping atoms are shown in gray.

t_D ($0.5 < \sigma_U < 1.7$ and $0.3 < \sigma_D < 1.7$) are the same order of magnitude for all examples of spiking / RTN, for all samples, and for all applied voltages / measured currents. This suggests that the distribution of pinning energies is similar in all cases, and that the same pinning energies are important for both filament formation and filament breaking. The width of the distribution of currents flowing in the UP state (see discussion of Figure S5 above) is also consistent with this model as it suggests modest variability in the positions of the key atoms in Figure 5b, and hence a variation in pinning energies.

The features described in the previous paragraph are broadly consistent with the model of Ref. 56, although we emphasize again that further experiments are required in order to allow a definitive conclusion as to whether atomic motion is driven by current or voltage. The strongly (weakly) exponential variation of τ_U (τ_D) with applied voltage is consistent with models in which the potential barriers for an atom to hop into (out of) the tunnel gap (Figure 5b) are highly asymmetric. In the present case it is clear that the barrier to hop out of the gap (i.e. to leave the UP conductance state) is much smaller, and hence the hopping rate $1/\tau_U$ is modified more strongly by the applied voltage. This type of asymmetry is discussed in some detail in Ref. 47, where it is also pointed out that the barrier heights may be affected by

15

charge states and redox processes. Hence, while these results provide important clues to the mechanism, detailed modeling is challenging – and made even more so by lack of knowledge of the local electric fields and currents within our percolating structures. It would be highly desirable in the future to study single tunnel junctions between tin particles, perhaps using similar methods to those employed for recent studies of Au break junctions.[57]

2.3 True Random Number Generation

We now show that the intrinsically stochastic nature of the spiking process can be exploited for true random number generation. A range of physical variables and nanoscale devices have previously been employed in TRNGs, as summarized in Section III of the Supporting Information. While impressive performance has been achieved, existing approaches suffer from various drawbacks (such as lack of compatibility with CMOS technologies, scalability, reliability, low bit rates and low technology readiness levels)[60,61] and alternative technologies are still required. In many cases additional post-processing steps are required to remove intrinsic bias in the underlying physical phenomena, *i.e.* in order to generate random numbers of sufficient quality for applications.

Here, we exploit the stochastic inter-spike intervals demonstrated in Figures 2d and f by converting them into random numbers. This approach provides significantly higher bit rates than alternative methods which convert the measured output currents (high or low) directly into bits (1s or 0s).[62] Figure 6a shows a schematic of a circuit that has been designed for this purpose, and Figure 6b shows the working principle. The current output of the device is fed into a spike detector comprising a high-pass filter, a comparator, a delay line and an AND gate. The output of the spike detector is an event train corresponding to the rising edges of the spikes. This event train is used to reset a multi-bit counter operating at a clock frequency set by an oscillator. (In our implementation the clock frequency is chosen to match the sampling speed of the measurement device.) The counter produces a binary number that encodes the time between spikes ($t_U + t_D$, middle panel of Figure 6b). Since
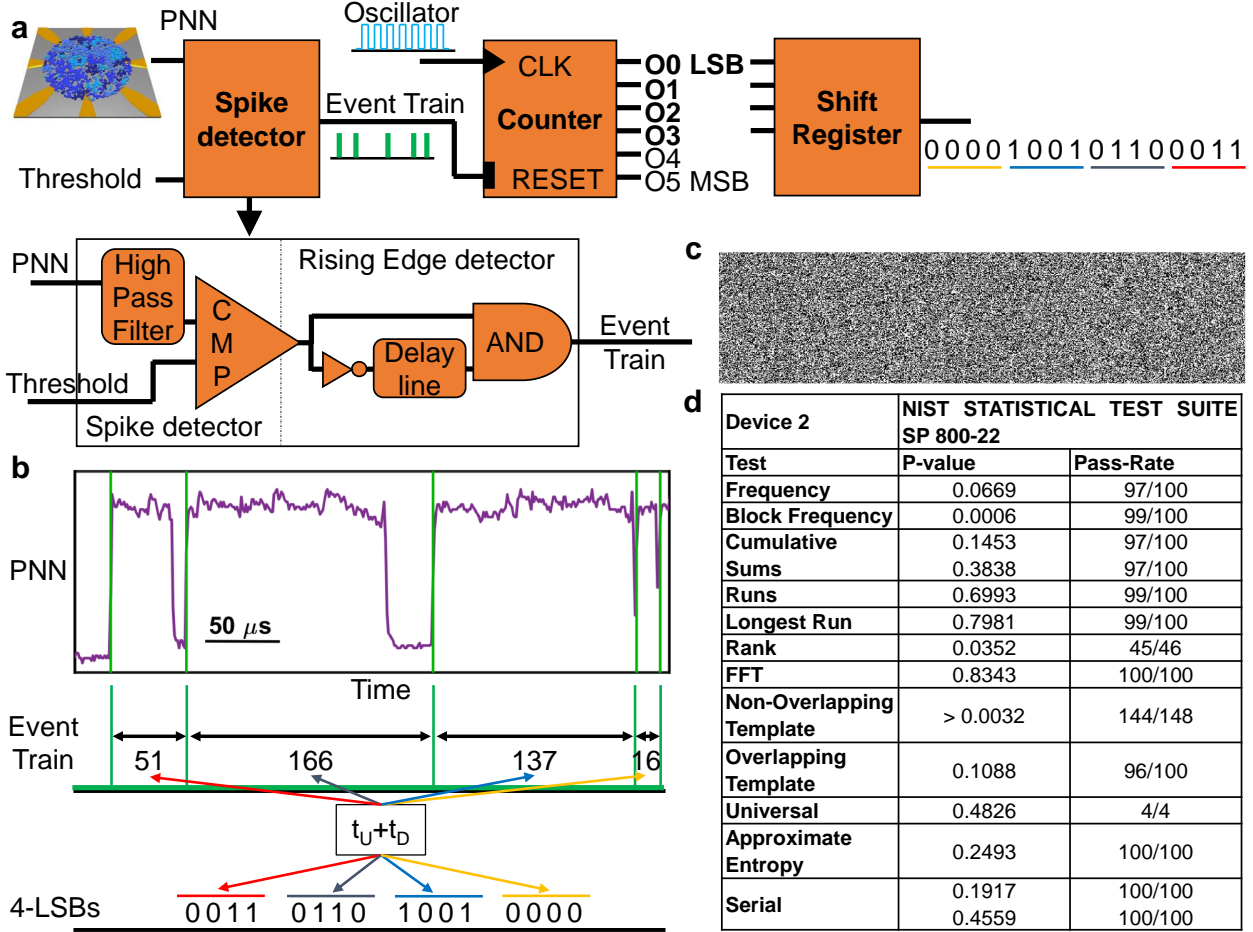
16

Figure 6: True Random Number Generator based on PNN. (a) Circuit schematic of the PNN-TRNG. The spiking output of the PNN is fed into a spike detector which generates an event train in correspondence with each rising edge. The event train is then fed into a multi-bit counter that operates at a frequency set by the oscillator and measures the time between rising step edges. The m least significant bits (LSBs) from the counter output, which are the most variable bits, are the inputs of a shift register which assembles the bits, generating the bit-stream. (b) Example of random number generation using data from Device 2 measured with a sampling interval of 1 μs. Each time between rising edges, $t_U + t_D$, is measured as a multiple of the oscillator period and subsequently converted to a binary number from which m LSBs are added to the bit-stream by the shift register. In this example 4 LSBs were selected. (c) Visual representation of a portion of a bit-stream generated using the PNN-TRNG. Each pixel represents a bit. White: ones, black: zeroes. (d) Results obtained from the NIST Statistical Test Suite SP 800-22.[59] The analyzed bit-stream was generated from 60 s of spiking activity obtained from Device 2 with a sampling interval of 1 μs, generating ~1.8 Mbits. 12 NIST tests were applied, carefully following the recommended protocols – see methods for details. Each test is considered passed, and the bit-stream is considered indistinguishable from a random one, if the pass rate is at least 96/100 and if p-value > 0.0001. Due to the limited number of sequences, the p-value reported for the universal test is the average of the p-values found for each sequence. The generated bit-stream from the proposed PNN-TRNG passes all the applied tests without the use of post-processing techniques.

the most significant bits change infrequently only the m least significant bits (LSBs) are retained,[31,62] as shown in the lower panel of Figure 6b. The best choice of m depends on the distribution of ISIs and generally needs to be tested experimentally. Finally, the output of the counter is converted into a bit-stream by a shift register.

Figure 6c illustrates a section of a generated random bit-stream. No obvious pattern is visible, suggesting that the bit-stream is at least qualitatively random. Detailed, quantitative testing of the quality of the bit-stream is achieved using the National Institute of Standards and Technology (NIST) Statistical Test Suite SP 800-22,[59] which was developed for precisely this purpose. The protocols suggested by NIST were followed carefully for each test. The tests return a pass rate and a p-value, and are considered passed if the pass rate is greater than 96/100 and if p-value > 0.0001. We found the best performance for $m = 4$, *i.e.* when the number of LSBs is chosen to correspond to the relatively flat part of the ISI histograms. This is consistent with previous reports that suggest that more uniform distributions are advantageous.[62] Note that the use of only the LSBs removes any possibility that serial correlations (Figure 3) affect the bit-stream.

We first tested our TRNG on datasets in which spiking is very homogeneous and well-resolved, measured with 10 μs sampling intervals. Figure S10 shows results obtained using part of the data presented in Figure 2. The overall bit rate is 16 kbits s^{-1} and the length of the generated bit-stream (800 kbits) is sufficient to apply 12 of 15 standard NIST tests. The bit-stream passes all 12 tests. When we tested longer datasets measured with the same sampling interval we found that they often failed the NIST frequency and cumulative sums tests. This is because the sampling interval is too long to completely resolve the spiking activity (the spike train is sub-sampled, see Figure S4b). More specifically, when the dataset includes many short ISIs, they cause biasing of the proportion of 1s and 0s.

In order to circumvent the sub-sampling issue we next tested the output of our TRNG using datasets which were measured using shorter (1 μs) sampling intervals. Figure 6d shows the test results generated from 60 s of spiking activity (data from Figure 6b). The overall

bit rate doubles to 30 kbits s^{-1}, the length of the bit-stream increases to $\sim$1.8 Mbits, and the bit-stream again passes all 12 of the 15 NIST tests for which sufficient data is available. Interestingly, this dataset includes segments of data where simultaneous spike trains from several tunnel gaps overlap (see Figure S9), and so Figure 6d shows that the output of the TRNG is robust, even for less homogeneous spiking. Hence, effective random number generation relies on high sampling speeds (to resolve the spikes) more than high homogeneity of the spiking sequences. A next step is to further increase the length of the bit-stream, but it would require approximately two orders of magnitude more data to attempt all 15 NIST tests, and new methods would be needed to handle the enormous datasets. Implementation of the TRNG in hardware would bypass these issues but would require major changes to our measurement and data acquisition systems. Careful design of the hardware should allow significant increases in clock speed and consequent improvements in the bit rate and length of bit-stream. The bit rate of the RNG mainly depends on mean of the ISI distribution and on the sampling interval. The bit rate could be improved significantly by moving to a faster measurement system that allows the sampling interval to be decreased. A further step would be to combine our device with a linear-feedback shift register (LFSR) which could increase the bit rate to $\sim$ 100 Mbits s^{-1}.[31]

Section III of the Supporting Information shows that the performance of our TRNG (bit rate, number of NIST tests passed, length of the tested bit-stream) is competitive with, and in many cases exceeds, that of most previously reported devices. In particular, Table S2 shows that our TRNG achieves high performance in all four key metrics. We emphasize that our TRNG passes all NIST tests for which there is sufficient data *without post-processing*. This means that the original spiking sequence is free of bias and that additional post-processing circuitry can be avoided. This is advantageous because post-processing is energy-intensive, reduces the final bit rate, and increases the total area of the device.

3   Conclusion

We have demonstrated that percolating networks of nanoparticles exhibit stochastic spiking behavior that is qualitatively similar to that observed for biological neurons. Spiking in our devices occurs on timescales that are about a thousand times faster than in the brain, providing opportunities for high-speed brain-like processing. Stochasticity is well-captured in histograms of inter-event intervals, and the observed log-normal distributions provide new insights into the atomic-scale switching mechanisms responsible for spiking. The spiking rate can be controlled via an input stimulus, similar to rate coding of information in biological systems. The combination of spiking activity (at local sites) and information processing capability (of the rest of the critical network)[36] has interesting parallels with biological recognition processes such as olfaction,[63] providing intriguing opportunities for development of novel neuromorphic systems. Finally, we showed that the stochastic behavior can be exploited for true random number generation and that high quality bit-streams can be generated, opening up opportunities for secure, brain-like information processing.

4   Methods

Device Fabrication

Our percolating devices are fabricated by simple nanoparticle deposition processes.[44,46,64] Multi-contact metal electrodes were fabricated using photolithographic processes, thermal evaporation, and lift-off techniques, on a Si wafer which has a 200 nm thick silicon nitride passivation layer. The metal electrodes are made of 5 nm of NiCr adhesion layer and 45 nm of Au. The electrodes are arranged around a circle of diameter of 600 μm. As described in detail in Refs. 36,44,46 a beam of particles is deposited on the devices in an UHV environment using electrical feedthroughs to enable the device conductance to be monitored during the deposition process. 7 nm Sn nanoparticles are deposited on the substrate and coalesce to form structures with a characteristic grain size of around 20 nm. Deposition is terminated at the onset of conduction, which corresponds to the percolation threshold.[64,65] The deposition takes place in a controlled environment with a well-defined partial pressure of air and humidity, as described in Ref. 46. This process leads to controlled coalescence and fabrication of robust structures which function for many months, but which yet allow atomic-scale switching processes to take place unhindered.[46]

Electrical Characterisation

Electrical measurements are carried out using a National Instruments multi-channel data acquisition system (NI PXIe-1082, PXIe-6378 ADC/DAC) and two distinct custom-developed sample mounting systems (SMS). One SMS has embedded trans-impedance amplifiers which transform the current measured through the device to measurable voltage outputs. The other SMS has push-pins which are the interface between the device and the external circuitry. In this case, series resistors are employed within the measurement circuit to measure the output currents. Electrical stimuli are applied to four opposite electrodes of the percolating device, while all other electrodes are grounded. DC measurements are used for the statistical analysis of spikes because they facilitate the observation of spikes for long

periods of time. Pulsed measurements are used to assess voltage dependent dynamics. The measurements reported here are performed with sampling intervals of either 1 μs or 10 μs.

Data Analysis

As described in detail in Ref. 36 the data analysis methods used in this work are substantially the same as those developed in the neuroscience community to analyze micro-electrode array recordings from biological brain tissue. Events are defined as changes in the current signal that exceed a threshold value. The data analysis is primarily performed in the MAT-LAB programming environment. We follow the maximum likelihood (ML) approach of Refs. 66,67 to estimate power-law, log-normal, and exponential fitting parameters for the IEI distributions and power-law fitting parameters for avalanche size and duration distributions.

Random Number Generation and NIST Randomness Tests

The working principle of the PNN-TRNG was analyzed in MATLAB on spike sequences measured using the same electrical characterization techniques described above. The NIST Statistical Test Suite was used to assess the randomness of the bit-stream.[59] The bit-stream is initially divided into sequences. Each test is then applied to each sequence and returns a p-value. The sequence passes the test if the p-value is greater than the significance level ($\alpha = 0.01$ for cryptographic applications as suggested in the NIST documentation). The statistical test suite returns a pass rate which is the proportion of how many sequences have passed the test. The pass rate must be greater than the pass rate threshold. Moreover, from the set of p-values found from testing the sequences, a second p-value is calculated to assess the uniformity of the p-values of the sequences. The bit-stream fully passes the tests of the NIST Statistical Tests Suite if and only if the pass rate is greater than the pass rate threshold and the second p-value is greater than 0.0001. In particular, all tests were run on 100 sequences of 18300 bits, except the rank test which was run on 46 sequences of 39000 bits and the universal test which was run on four sequences of 450000 bits for data measured from Device 2 with a sampling interval of 1 μs.

4.1 Supporting Information

The Supporting Information is available free of charge on the ACS Publications website at DOI: *******.

(Figure S1) Images of a PNN device; (Figure S2) Inter-event intervals, and avalanche and criticality analyses; (Figure S3) Examples of spiking activity measured with 1 μs sampling interval; (Figure S4) Examples of spiking activity measured with 10 μs sampling interval; (Figure S5) Histograms of the measured current for the segment of data from Device 1 shown in Figure 2a; (Figure S6) Histogram of the ISIs for the dataset used in Figure 3; (Figure S7) Analysis of data from Figure 4 of the main text using a standard methodology for random telegraph noise (RTN); (Table S1) Summary of the analyzed sequences of data from three different devices; (Figure S8) Variation of the mean times in the UP and DOWN states. τ_U (panel a) and τ_D (panel b) are plotted against the ratio τ_U/τ_D for all the spiking data of different devices; (Figure S9) Examples of detected rising edges of spikes using the TRNG circuit, showing robustness of the method; (Figure S10) True Random Number Generation from data measured with a sampling interval of 10 μs. (Figure S11) Stochasticity and serial correlations. Reproduction for the reader's convenience of Figure 3 from the main text; (Table S2) Comparison of TRNG performance with results from the literature.

4.2 Author Contributions

S.A.B conceived the study and initiated the project. S.K.A and E.G contributed equally to this work. S.K.A, E.G, J.B.M. and F.W. performed experiments and associated data analysis. J.B.M., Z.H., P.B., M.D.A. performed simulations. S.A.B., S.K.A., and E.G. wrote the manuscript with comments from all authors.

4.3 Notes

The authors declare that they have no competing financial interests.

Acknowledgement

References

(1) Marković, D.; Mizrahi, A.; Querlioz, D.; Grollier, J. Physics for Neuromorphic Computing. *Nature Reviews Physics* **2020**, *2*, 499–510.

(2) Zhao, M.; Gao, B.; Tang, J.; Qian, H.; Wu, H. Reliability of Analog Resistive Switching Memory for Neuromorphic Computing. *Applied Physics Reviews* **2020**, *7*, 011301.

(3) Krestinskaya, O.; James, A. P.; Chua, L. O. Neuromemristive Circuits for Edge Computing: A Review. *IEEE Transactions on Neural Networks and Learning Systems* **2020**, *31*, 4–23.

(4) Wang, J.; Zhuge, F. Memristive Synapses for Brain-Inspired Computing. *Advanced Materials Technologies* **2019**, *4*, 1800544.

(5) Wang, L.; Liao, W.; Wong, S. L.; Yu, Z. G.; Li, S.; Lim, Y.-F.; Feng, X.; Tan, W. C.; Huang, X.; Chen, L.; Liu, L.; Chen, J.; Gong, X.; Zhu, C.; Liu, X.; Zhang, Y.-W.; Chi, D.; Ang, K.-W. Artificial Synapses Based on Multiterminal Memtransistors for Neuromorphic Application. *Advanced Functional Materials* **2019**, *29*, 1901106.

(6) Jiang, J.; Guo, J.; Wan, X.; Yang, Y.; Xie, H.; Niu, D.; Yang, J.; He, J.; Gao, Y.; Wan, Q. 2D MoS 2 Neuromorphic Devices for Brain-Like Computational Systems. *Small* **2017**, *13*, 1700933.

(7) Ambrogio, S.; Ciocchini, N.; Laudato, M.; Milo, V.; Pirovano, A.; Fantini, P.; Ielmini, D. Unsupervised Learning by Spike Timing Dependent Plasticity in Phase Change Memory (PCM) Synapses. *Frontiers in Neuroscience* **2016**, *10*, 56.

(8) Mahowald, M.; Douglas, R. A Silicon Neuron. *Nature* **1991**, *354*, 515–518.

(9) Merolla, P. A.; Arthur, J. V.; Alvarez-Icaza, R.; Cassidy, A. S.; Sawada, J.; Akopyan, F.; Jackson, B. L.; Imam, N.; Guo, C.; Nakamura, Y.; Brezzo, B.; Vo, I.; Esser, S. K.; Appuswamy, R.; Taba, B.; Amir, A.; Flickner, M. D.; Risk, W. P.; Manohar, R.;

Modha, D. S. A Million Spiking-Neuron Integrated Circuit with a Scalable Communication Network and Interface. *Science* **2014**, *345*, 668–673.

(10) Furber, S. Large-Scale Neuromorphic Computing Systems. *Journal of Neural Engineering* **2016**, *13*, 051001.

(11) Pickett, M. D.; Medeiros-Ribeiro, G.; Williams, R. S. A Scalable Neuristor Built with Mott Memristors. *Nature Materials* **2013**, *12*, 114–117.

(12) Kumar, S.; Williams, R. S.; Wang, Z. Third-Order Nanocircuit Elements for Neuromorphic Engineering. *Nature* **2020**, *585*, 518–523.

(13) Wang, Z.; Joshi, S.; Savel'ev, S.; Song, W.; Midya, R.; Li, Y.; Rao, M.; Yan, P.; Asapu, S.; Zhuo, Y.; Jiang, H.; Lin, P.; Li, C.; Yoon, J. H.; Upadhyay, N. K.; Zhang, J.; Hu, M.; Strachan, J. P.; Barnell, M.; Wu, Q.; Wu, H.; Williams, R. S.; Xia, Q.; Yang, J. J. Fully Memristive Neural Networks for Pattern Classification with Unsupervised Learning. *Nature Electronics* **2018**, *1*, 137–145.

(14) Stoliar, P.; Tranchant, J.; Corraze, B.; Janod, E.; Besland, M.-P.; Tesler, F.; Rozenberg, M.; Cario, L. A Leaky-Integrate-and-Fire Neuron Analog Realized with a Mott Insulator. *Advanced Functional Materials* **2017**, *27*, 1604740.

(15) Wang, Z.; Rao, M.; Han, J.-W.; Zhang, J.; Lin, P.; Li, Y.; Li, C.; Song, W.; Asapu, S.; Midya, R.; Zhuo, Y.; Jiang, H.; Yoon, J. H.; Upadhyay, N. K.; Joshi, S.; Hu, M.; Strachan, J. P.; Barnell, M.; Wu, Q.; Wu, H.; Qiu, Q.; Williams, R. S.; Xia, Q.; Yang, J. J. Capacitive Neural Network with Neuro-Transistors. *Nature Communications* **2018**, *9*, 3208.

(16) Tuma, T.; Pantazi, A.; Le Gallo, M.; Sebastian, A.; Eleftheriou, E. Stochastic Phase-Change Neurons. *Nature Nanotechnology* **2016**, *11*, 693–699.

(17) Gao, L.; Chen, P.-Y.; Yu, S. NbOx Based Oscillation Neuron for Neuromorphic Computing. *Applied Physics Letters* **2017**, *111*, 103503.

(18) Ignatov, M.; Ziegler, M.; Hansen, M.; Petraru, A.; Kohlstedt, H. A Memristive Spiking Neuron with Firing Rate Coding. *Frontiers in Neuroscience* **2015**, *9*, 1–9.

(19) Franke, F.; Fiscella, M.; Sevelev, M.; Roska, B.; Hierlemann, A.; Azeredo da Silveira, R. Structures of Neural Correlation and How They Favor Coding. *Neuron* **2016**, *89*, 409–422.

(20) Stein, R. B.; Gossen, E. R.; Jones, K. E. Neuronal Variability: Noise or Part of the Signal? *Nature Reviews Neuroscience* **2005**, *6*, 389–397.

(21) McDonnell, M. D.; Ward, L. M. The Benefits of Noise in Neural Systems: Bridging Theory and Experiment. *Nature Reviews Neuroscience* **2011**, *12*, 415–425.

(22) Branco, T.; Staras, K. The Probability of Neurotransmitter Release: Variability and Feedback Control at Single Synapses. *Nature Reviews Neuroscience* **2009**, *10*, 373–383.

(23) Hamilton, T. J.; Afshar, S.; van Schaik, A.; Tapson, J. Stochastic Electronics: A Neuro-Inspired Design Paradigm for Integrated Circuits. *Proceedings of the IEEE* **2014**, *102*, 843–859.

(24) Shim, Y.; Jaiswal, A.; Roy, K. Ising Computation Based Combinatorial Optimization Using Spin-Hall Effect (SHE) Induced Stochastic Magnetization Reversal. *Journal of Applied Physics* **2017**, *121*, 193902.

(25) Maass, W. To Spike or Not to Spike: That Is the Question. *Proceedings of the IEEE* **2015**, *103*, 2219–2224.

(26) Yang, K.; Duan, Q.; Wang, Y.; Zhang, T.; Yang, Y.; Huang, R. Transiently Chaotic Simulated Annealing Based on Intrinsic Nonlinearity of Memristors for Efficient Solution of Optimization Problems. *Science Advances* **2020**, *6*, eaba9901.

(27) Jonke, Z.; Habenschuss, S.; Maass, W. Solving Constraint Satisfaction Problems with Networks of Spiking Neurons. *Frontiers in Neuroscience* **2016**, *10*, 1–16.

(28) Mahmoodi, M. R.; Prezioso, M.; Strukov, D. B. Versatile Stochastic Dot Product Circuits Based on Nonvolatile Memories for High Performance Neurocomputing and Neurooptimization. *Nature Communications* **2019**, *10*, 5113.

(29) Cai, F.; Kumar, S.; Van Vaerenbergh, T.; Sheng, X.; Liu, R.; Li, C.; Liu, Z.; Foltin, M.; Yu, S.; Xia, Q.; Yang, J. J.; Beausoleil, R.; Lu, W. D.; Strachan, J. P. Power-Efficient Combinatorial Optimization using Intrinsic Noise in Memristor Hopfield Neural Networks. *Nature Electronics* **2020**, *3*, 409–418.

(30) Carboni, R.; Ielmini, D. Stochastic Memory Devices for Security and Computing. *Advanced Electronic Materials* **2019**, *5*, 1900198.

(31) Jiang, H.; Belkin, D.; Savel'ev, S. E.; Lin, S.; Wang, Z.; Li, Y.; Joshi, S.; Midya, R.; Li, C.; Rao, M.; Barnell, M.; Wu, Q.; Yang, J. J.; Xia, Q. A Novel True Random Number Generator Based on a Stochastic Diffusive Memristor. *Nature Communications* **2017**, *8*, 882.

(32) Click, T. H.; Liu, A.; Kaminski, G. A. Quality of Random Number Generators Significantly Affects Results of Monte Carlo Simulations for Organic and Biological Systems. *Journal of Computational Chemistry* **2011**, *32*, 513–524.

(33) Sebastian, A.; Le Gallo, M.; Khaddam-Aljameh, R.; Eleftheriou, E. Memory Devices and Applications for in-Memory Computing. *Nature Nanotechnology* **2020**, *15*, 529–544.

(34) Herrero-Collantes, M.; Garcia-Escartin, J. C. Quantum Random Number Generators. *Reviews of Modern Physics* **2017**, *89*, 015004.

(35) Matsumoto, M.; Nishimura, T. Mersenne Twister: A 623-Dimensionally Equidistributed Uniform Pseudo-Random Number Generator. *ACM Transactions on Modeling and Computer Simulation* **1998**, *8*, 3–30.

(36) Mallinson, J. B.; Shirai, S.; Acharya, S. K.; Bose, S. K.; Galli, E.; Brown, S. A. Avalanches and Criticality in Self-Organized Nanoscale Networks. *Science Advances* **2019**, *5*, eaaw8438.

(37) Shirai, S.; Acharya, S. K.; Bose, S. K.; Mallinson, J. B.; Galli, E.; Pike, M. D.; Arnold, M. D.; Brown, S. A. Long-Range Temporal Correlations in Scale-Free Neuromorphic Networks. *Network Neuroscience* **2020**, *4*, 432–447.

(38) Pike, M. D.; Bose, S. K.; Mallinson, J. B.; Acharya, S. K.; Shirai, S.; Galli, E.; Weddell, S. J.; Bones, P. J.; Arnold, M. D.; Brown, S. A. Atomic Scale Dynamics Drive Brain-like Avalanches in Percolating Nanostructured Networks. *Nano Letters* **2020**, *20*, 3935–3942.

(39) Milano, G.; Pedretti, G.; Fretto, M.; Boarino, L.; Benfenati, F.; Ielmini, D.; Valov, I.; Ricciardi, C. Brain-Inspired Structural Plasticity through Reweighting and Rewiring in Multi-Terminal Self-Organizing Memristive Nanowire Networks. *Advanced Intelligent Systems* **2020**, *2*, 2000096.

(40) Demis, E. C.; Aguilera, R.; Scharnhorst, K.; Aono, M.; Stieg, A. Z.; Gimzewski, J. K. Nanoarchitectonic Atomic Switch Networks for Unconventional Computing. *Japanese Journal of Applied Physics* **2016**, *55*, 1102B2.

(41) Manning, H. G.; Niosi, F.; da Rocha, C. G.; Bellew, A. T.; O'Callaghan, C.; Biswas, S.; Flowers, P. F.; Wiley, B. J.; Holmes, J. D.; Ferreira, M. S.; Boland, J. J. Emergence of Winner-Takes-All Connectivity Paths in Random Nanowire Networks. *Nature Communications* **2018**, *9*, 3219.
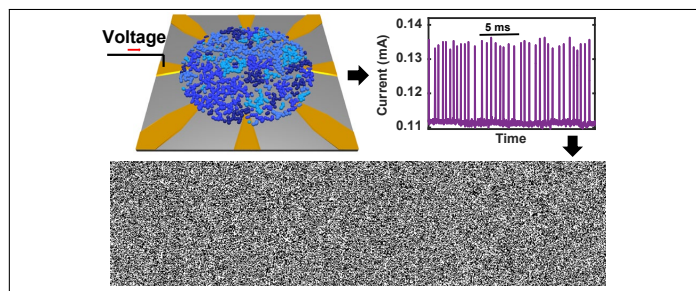
(42) Kuncic, Z.; Nakayama, T. Neuromorphic Nanowire Networks: Principles, Progress and Future Prospects for Neuro-Inspired Information Processing. *Advances in Physics: X* **2021**, *6*, 1894234.

(43) Mirigliano, M.; Borghi, F.; Podestà, A.; Antidormi, A.; Colombo, L.; Milani, P. Non-ohmic Behavior and Resistive Switching of Au Cluster-assembled Films Beyond the Percolation Threshold. *Nanoscale Advances* **2019**, *1*, 3119–3130.

(44) Sattar, A.; Fostner, S.; Brown, S. A. Quantized Conductance and Switching in Percolating Nanoparticle Films. *Physical Review Letters* **2013**, *111*, 136808.

(45) Terabe, K.; Hasegawa, T.; Nakayama, T.; Aono, M. Quantized Conductance Atomic Switch. *Nature* **2005**, *433*, 47–50.

(46) Bose, S. K.; Mallinson, J. B.; Gazoni, R. M.; Brown, S. A. Stable Self-Assembled Atomic-Switch Networks for Neuromorphic Applications. *IEEE Transactions on Electron Devices* **2017**, *64*, 5194–5201.

(47) Soni, R.; Meuffels, P.; Petraru, A.; Weides, M.; Kügeler, C.; Waser, R.; Kohlstedt, H. Probing Cu Doped Ge0.3Se0.7 Based Resistance Switching Memory Devices with Random Telegraph Noise. *Journal of Applied Physics* **2010**, *107*, 024517.

(48) Kish, E. A.; Granqvist, C.-G.; Dér, A.; Kish, L. B. Lognormal Distribution of Firing Time and Rate from a Single Neuron? *Cognitive Neurodynamics* **2015**, *9*, 459–462.

(49) Song, S.; Lee, J. A.; Kiselev, I.; Iyengar, V.; Trapani, J. G.; Tania, N. Mathematical Modeling and Analyses of Interspike-Intervals of Spontaneous Activity in Afferent Neurons of the Zebrafish Lateral Line. *Scientific Reports* **2018**, *8*, 14851.

(50) Farkhooi, F.; Strube-Bloss, M. F.; Nawrot, M. P. Serial Correlation in Neural Spike Trains: Experimental Evidence, Stochastic Modeling, and Single Neuron Variability. *Physical Review E* **2009**, *79*, 021905.

(51) Karpov, V. G.; Niraula, D. Log-Normal Statistics in Filamentary RRAM Devices and Related Systems. *IEEE Electron Device Letters* **2017**, *38*, 1240–1243.

(52) Feali, M. S.; Ahmadi, A. Realistic Hodgkin-Huxley Axons Using Stochastic Behavior of Memristors. *Neural Processing Letters* **2017**, *45*, 1–14.

(53) Medeiros-Ribeiro, G.; Perner, F.; Carter, R.; Abdalla, H.; Pickett, M. D.; Williams, R. S. Lognormal Switching Times for Titanium Dioxide Bipolar Memristors: Origin and Resolution. *Nanotechnology* **2011**, *22*, 095702.

(54) Pickett, M. D.; Strukov, D. B.; Borghetti, J. L.; Yang, J. J.; Snider, G. S.; Stewart, D. R.; Williams, R. S. Switching Dynamics in Titanium Dioxide Memristive Devices. *Journal of Applied Physics* **2009**, *106*, 074508.

(55) Yu, S.; Wong, H.-S. P. Compact Modeling of Conducting-Bridge Random-Access Memory (CBRAM). *IEEE Transactions on Electron Devices* **2011**, *58*, 1352–1360.

(56) Schirm, C.; Matt, M.; Pauly, F.; Cuevas, J. C.; Nielaba, P.; Scheer, E. A Current-Driven Single-Atom Memory. *Nature Nanotechnology* **2013**, *8*, 645–648.

(57) Wang, Q.; Liu, R.; Xiang, D.; Sun, M.; Zhao, Z.; Sun, L.; Mei, T.; Wu, P.; Liu, H.; Guo, X.; Li, Z.-L.; Lee, T. Single-Atom Switches and Single-Atom Gaps Using Stretched Metal Nanowires. *ACS Nano* **2016**, *10*, 9695–9702.

(58) Ring, M.; Weber, D.; Haiber, P.; Pauly, F.; Nielaba, P.; Scheer, E. Voltage-Induced Rearrangements in Atomic-Size Contacts. *Nano Letters* **2020**, *20*, 5773–5778.

(59) Rukhin, A.; Soto, J.; Nechvatal, J.; Smid, M.; Leigh, S.; Levenson, M.; Vangel, M.; Banks, D.; Heckert, A.; Dray, J.; Vo, S.; Bassham, L. *A Statistical Test Suite for Random and Pseudorandom Number Generators for Cryptographic Applications*; Special Publication (NIST SP 800-22 Rev. 1a), National Institute of Standards and Technology, Gaithersburg, MD, 2010.

(60) Woo, K. S.; Wang, Y.; Kim, J.; Kim, Y.; Kwon, Y. J.; Yoon, J. H.; Kim, W.; Hwang, C. S. A True Random Number Generator using Threshold-Switching-Based Memristors in an Efficient Circuit Design. *Advanced Electronic Materials* **2019**, *5*, 1800543.

(61) Wen, C.; Li, X.; Zanotti, T.; Puglisi, F. M.; Shi, Y.; Saiz, F.; Antidormi, A.; Roche, S.; Zheng, W.; Liang, X.; Hu, J.; Duhm, S.; Roldan, J. B.; Wu, T.; Chen, V.; Pop, E.; Garrido, B.; Zhu, K.; Hui, F.; Lanza, M. Advanced Data Encryption using 2D Materials. *Advanced Materials* **2021**, *33*, 2100185.

(62) Chen, X.; Li, B.; Wang, Y.; Liu, Y.; Yang, H. A Unified Methodology for Designing Hardware Random Number Generators Based on any Probability Distribution. *IEEE Transactions on Circuits and Systems II: Express Briefs* **2016**, *63*, 783–787.

(63) Niessing, J.; Friedrich, R. W. Olfactory Pattern Classification by Discrete Neuronal Network States. *Nature* **2010**, *465*, 47–52.

(64) Schmelzer, J.; Brown, S. A.; Wurl, A.; Hyslop, M.; Blaikie, R. J. Finite-Size Effects in the Conductivity of Cluster Assembled Nanostructures. *Physical Review Letters* **2002**, *88*, 226802.

(65) Stauffer, D.; Aharony, A. *Introduction to Percolation Theory*, 2nd ed.; CRC Press, New York, 1992.

(66) Clauset, A.; Shalizi, C. R.; Newman, M. E. J. Power-Law Distributions in Empirical Data. *SIAM Review* **2009**, *51*, 661–703.

(67) Deluca, A.; Corral, Á. Fitting and Goodness-of-fit Test of Non-truncated and Truncated Power-law Distributions. *Acta Geophysica* **2013**, *61*, 1351–1394.

Graphical TOC Entry

For Table of Contents Only